ARTICLE OPEN

Check for updates

An intrinsically stretchable multi-biochemical sensor for sweat analysis using photo-patternable ecoflex

Seungwan Kim[1,2], Joohyuk Kang[3], Injun Lee[1,2], Jinhyeong Jang[2], Chan Beum Park[2], Wonryung Lee[3]✉ and Byeong-Soo Bae[1,2]✉

Ecoflex is widely used in bioelectronics due to its outstanding properties of low modulus and large stretchability. For its use as an encapsulation layer in multi-channel wearable devices, a patterning procedure is essential. However, conventional patterning strategies for Ecoflex, such as soft lithography, punching, and laser ablation, lack sufficient quality and process compatibility. To address this, we propose a process-compatible method of patterning Ecoflex by developing Photo-patternable Ecoflex (PPE). The PPE layer, used as an encapsulation layer, effectively dissipates strain energy at homogeneous interfaces, resulting in a 50% increase in electrical conductance under 250% strain. Using PPE, we fabricated intrinsically stretchable multi-sensors that monitor bio-signals like glucose, lactate, pH, and humidity in sweat. These sensors maintain durable sensitivity under strain up to 50% and for 1000 cycles at 20% strain. Finally, we mounted these stretchable multi-chemical sensors on an arm to monitor glucose and lactate levels in sweat.

npj Flexible Electronics (2023)7:33 ; https://doi.org/10.1038/s41528-023-00268-x

INTRODUCTION

An encapsulation layer is one of the most important layers in flexible bioelectronics for preventing the degradation and oxidization of circuit components from fluids and ions[1–4]. It also functions as an adhesive layer between human tissue and flexible electronics[5]. To use such a layer at a bio-interface for monitoring biological signals, the encapsulation layer should be patterned to create an open window to directly detect analytes[6–9]. Organic polymers, including polyimide, parylene, and SU8, which are widely used in flexible electronics as encapsulation materials, can be patterned through photolithography and reactive ion etching with systematic alignment[10,11].

Currently, stretchable materials such as poly(dimethylsiloxane) (PDMS)[12–14], styrene ethylene/butylene styrene (SEBS)[15–17], and Ecoflex[18–20] have been utilized to enhance the wearing comfort and reliability in flexible electronics. These materials, notable for their stretchability, facilitate the collection of biochemical data from specific target areas without causing discomfort or interruptions[21–26]. In previous studies, wearable sensor that combines silicone-derived elastomers with carbon nanotube (CNTs) and Au nanosheet has been developed, demonstrating a stretchability up to 30%[27]. Additionally, a stretchable multimodal sensing patch utilizing a copolymer (e.g., styrene-butadiene-styrene block copolymer) was shown to monitor blood pressure and biomarkers in sweat and interstitial fluid (ISF) at a 20% strain[28].

Stretchable materials are commonly patterned by soft lithography, laser ablation or punching, but an additional lamination process on the circuit is required[29–32]. Furthermore, theses conventional patterning methods have been shown to be time-consuming with low yield. Thus, it is still necessary to establish a systematic aligning method in stretchable electronics for making large area, sophisticated, and multi-functional sensors. An alternative patterning approach is to endow photo-patternability to stretchable materials[33]. For example, photo-patternable PDMS, applied to an encapsulation layer of a stretchable organic electrochemical transistor (OECT), provided a window for electrocardiographic (ECG) monitoring[34]. Also, it was used to fabricate a mechanically heterogeneous substrate for a strain sensor with tunable mechanical properties[35].

While photo-patternable PDMS has been previously demonstrated, Ecoflex offers distinct advantages and features that make it a valuable material for wearable biosensors. With an elastic stretchability of over 1000% and a modulus in the kilo-Pascal range, Ecoflex closely matches the mechanical properties of human skin[36]. This exceptional stretchability and deformability enable a more comfortable integration of biosensors into wearable devices, minimizing the impact of body movement on device performance. Ecoflex's high elasticity and deformability also help maintain the structural integrity of the biosensor during repeated stretching and bending. It can undergo reversible deformation without permanent damage, ensuring the longevity and durability of the device[18–20]. However, a highly process-compatible patterning method for Ecoflex has not yet been developed owing to its short pot life compared to that of PDMS. As Ecoflex is rapidly cured even at room temperature, it is challenging to control the photo-patterning process.

To address this challenge, we have developed Photo-patternable Ecoflex (PPE), which include curing retarder and a photo-inhibitor. This incorporation extends the pot life of the material and ensures compatibility with the manufacturing process. PPE allows for the direct creation of multi-windows in a process-compatible manner, enabling the fabrication of large-area, sophisticated, and multi-functional sensors. We integrated PPE with a stretchable silver (Ag) composite, forming an encapsulation layer through a direct patterning process. The homogeneous interface between the encapsulation and conductor contributes to efficient strain energy dissipation, at 250% strain, stretchable electrodes with PPE encapsulation showed 50%

[1]Wearable Platform Materials Technology Center (WMC), 291 Daehak-ro, Yuseong-gu, Daejeon 34141, Republic of Korea. [2]Department of Materials Science and Engineering, Korea Advanced Institute of Science and Technology (KAIST), 291 Daehak-ro, Yuseong-gu, Daejeon 34141, Republic of Korea. [3]Center for Theragnosis, Biomedical Research Institute, KIST, Seoul 02792, Republic of Korea. ✉email: wrlee@kist.re.kr; bsbae@kaist.ac.kr

higher electrical conductance than stretchable electrodes without PPE encapsulation. Moreover, to increase electrical stability under sweating conditions where human skin is directly exposed to the stretchable electrode, we used a galvanic replacement process to form gold nanoparticles (AuNPs) on Ag flakes[37,38]. By integration of the developed PPE, we fabricated an intrinsically-stretchable device for multiple chemical targets such as humidity, pH, glucose and lactate. Finally, this sensor was used to continuously monitor the glucose and lactate levels in human sweat. The glucose level was quantified as 70 mg/dL during fasting, and 100 mg/dL after food intake. The lactate level was estimated as 5 mM–16 mM during exercise. These results were comparable with those of commercial essay kits for glucose and lactate.

RESULTS AND DISCUSSION

Photo-patternable Ecoflex as an encapsulation of the silver stretchable conductor

We modified Ecoflex to respond to ultraviolet (UV) light for direct photo-patterning by adding benzophenone. Ecoflex is a silicone elastomers that is normally cured by thermal energy, but the addition of benzophenone as a photo-initiator allows it to respond to UV exposure (Fig. 1a–i)[33,39]. UV light induces the formation of benzophenone free radicals, which prevent the polymerization of Ecoflex by reacting with uncured Ecoflex. After UV exposure, the exposed Ecoflex remains uncured due to the radical reaction with the benzophenone radicals, while the unexposed Ecoflex polymerizes during the pre-bake. Therefore, the exposed region can be removed by the developer, whereas the cured unexposed areas remain (Fig. 1a-ii, iii). The absorption spectrum of benzophenone peaks at wavelength $\lambda = 260$ nm with a tail at $\lambda = 365$ nm, so PPE is only responsive to light that has $\lambda < 365$ nm[40]. Benzophenone radicals are not hindered by atmospheric oxygen, so PPE could be patterned in ambient air. The desired star shape of the hole was formed by direct photo-patterning of PPE on the Ecoflex substrate (Fig. 1b). The multi-layered Ecoflex was stretched 200% without tearing or delaminating. PPE layer could be patterned into holes in circles and squares in sizes from 1000 to 250 µm (Supplementary Fig. 1). The minimum achievable resolution of the patterned PPE is estimated to be approximately 200 µm. We also verified the non-cytotoxicity of PPE through in vitro biocompatibility test using mouse skin cells. Detail of the experiment is shown in Supplementary Fig. 2.

The Ecoflex surrounded the stretchable conductor (Supplementary Fig. 3). To identify how the stretchable nanocomposite combined with Ag flakes behaves under strain, its surface morphology was visualized using by 3D laser microscopy before and after stretching to 100% (Fig. 1c). 3D laser microscopy can observe the behavior of the Ag nanocomposite located between the modified Ecoflex substrate and the encapsulation layer. According to percolation theory, the conductivity of a stretchable nanocomposite is related to a percolation pathway[41–43]. When the non-encapsulated nanocomposite was stretched to 100%, its surface roughness increased to induce long percolation pathways and local micro-cracks that degrade the conductivity of the nanocomposite (Fig. 1c). In contrast, the nanocomposite covered by PPE withstood the applied strain without change in surface roughness; this resiliency is a result of the dense linking that the direct patterning process induces between the substrate and encapsulation layer. By integration of PPE as the encapsulation for the stretchable conductor, the roughness of the conductor is maintained so that PPE could increase the conductor's tolerance of mechanical deformation.

We evaluated how the PPE encapsulation layer affected the electrical properties of the stretchable conductor. When stretched up to 250% strain, its normalized resistance varied. The encapsulated stretchable conductor exhibited stable electrical characteristics under 250% strain, whereas those of the non-encapsulated conductor degraded (Fig. 1d). Furthermore, electrical characteristics of the encapsulated stretchable conductor were retained after 1,000 cycles of repetitive deformation at 100% strain (Fig. 1e). Also we compared mechanical and electrical characteristics of electrodes between PDMS-based electrode and an Ecoflex-based electrode encapsulated with PPE (Supplementary Fig. 4). PPE also displayed high elongation (i.e., >800%) and a slightly increased tensile strength compared to Ecoflex. The adhesive strength of PDMS, Ecoflex, and PPE was evaluated. Adhesive strength refers to the property associated with tackiness, which describes a material's ability to adhere to surfaces. In comparison, PDMS exhibited lower tackiness compared to PPE. The normalized resistance of the electrode made with Ecoflex and PPE demonstrates a linear increase that is proportional to strain. In contrast, the electrode made with PDMS shows a rapid increase in resistance beyond the elastic region. Furthermore, at 50% strain, the conductivity of the Ecoflex-based electrode is 60% higher than that of the PDMS-based electrode.

Modification of Ag electrode by galvanic coating process

Biochemical sensors rely on the contact interfaces to function effectively on soft biological surfaces. However, exposing the Ag-based nanocomposite conductor to skin may lead to skin irritation and device instability due to its tendency to oxidize during sweating. To enhance biocompatibility and electrochemical characteristics of Ag electrode, we deposited gold nanoparticles (AuNPs) on Ag flakes through a galvanic replacement process. This process is a spontaneous reaction between the Ag flake and $AuCl^{4-}$(aq)[30]. The AuNPs are non-toxic and have high resistance to oxidation, which improves the biocompatibility and electrochemical characteristics of the electrodes[44,45]. The Ag nanocomposite was coated with AuNPs through the galvanic replacement process after direct photo-patterning of the PPE[37,46]. Energy-dispersive X-ray spectroscopy (EDS) images show uniformly-dispersed AuNPs on the Ag flakes (Fig. 2b–d). Gold nanoparticles (AuNPs) possess a spherical structure, as shown in Supplementary Fig. 5. The growth of these nanoparticles onto the silver flakes was observed to be random. The size of the gold nanoparticles ranges between approximately 100 and 200 nanometers. The electrochemical properties of the Au-modified Ag electrode were characterized and compared with a bare Ag electrode. Cyclic voltammetry (CV) plots show larger electrical current amplitudes and sharper peaks on the Au-modified Ag electrode than on the bare Ag electrode during electrodeposition of Prussian Blue (PB) (Fig. 2e). A thinner Prussian blue layer is deposited to achieve better sensitivity for accurate low-glucose-level measurements in sweat. On the other hand, for lactate sensors, the thicker Prussian blue layer was deposited onto the electrodes[21,47] (Supplementary Fig. 6). A redox peak is noticed between 0.1–0.2 V, signifying that the redox reactions happening at the electrode are reversible. Furthermore, when an electrode with AuNPs is used, the redox reaction is more distinct compared to the bare silver electrode. (Fig. 2f). Coating of the Ag electrode with AuNPs increased its electrochemical properties, including a decrease in the interfacial impedance of PEDOT (Supplementary Figs. 7, 2g). Likewise, platinum nanoparticles (PtNPs) were deposited onto the Ag nanocomposite for counter electrode by galvanic replacement process (Supplementary Fig. 8) since platinum is highly stable, inert, and resistant to oxidation, making it ideal for long-term stability and consistent performance as a counter electrode[48].

Device design strategies for an intrinsically stretchable multi chemical sensor

The wearable biochemical sensing patch (Fig. 3a) was made stretchable by incorporating intrinsically stretchable materials

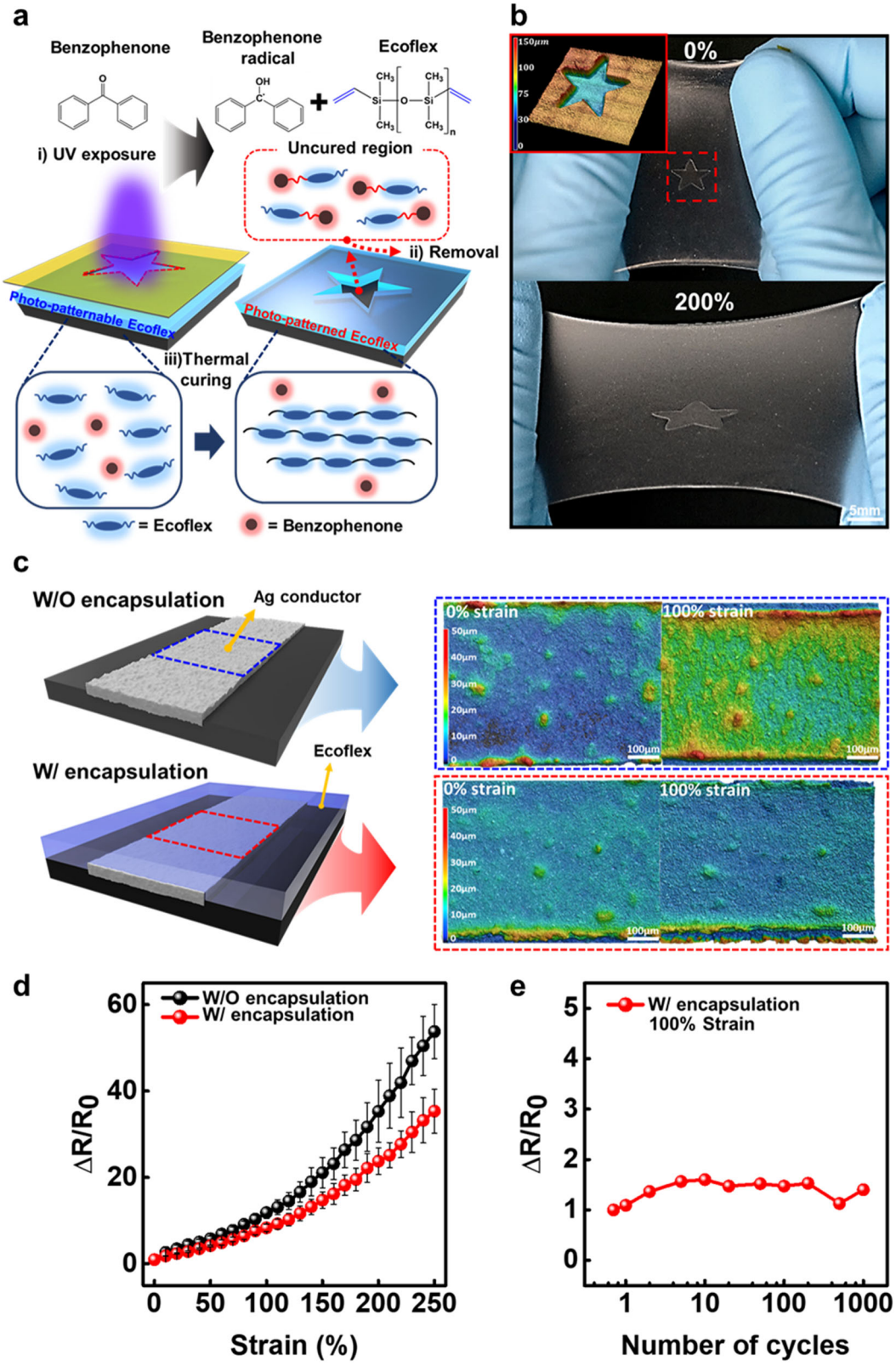

Fig. 1 Intrinsically stretchable electrode using Ag flake encapsulated by Photo-patternable Ecoflex. a Schematic illustration of photo-patterning process using Photo-patternable Ecoflex (PPE) **b** Photograph of photo-patterned Ecoflex as a star shape on Ecoflex substrate when stretched up to 200%. **c** 3D laser microscope image of cross-section of electrode layers. **d** Normalized resistance comparison of the electrode with and without Ecoflex encapsulation layer. Data are presented as mean ± SD. ($n = 3$) **e** Normalized resistance of the encapsulated electrode after 1000 cycles at 100% strain.

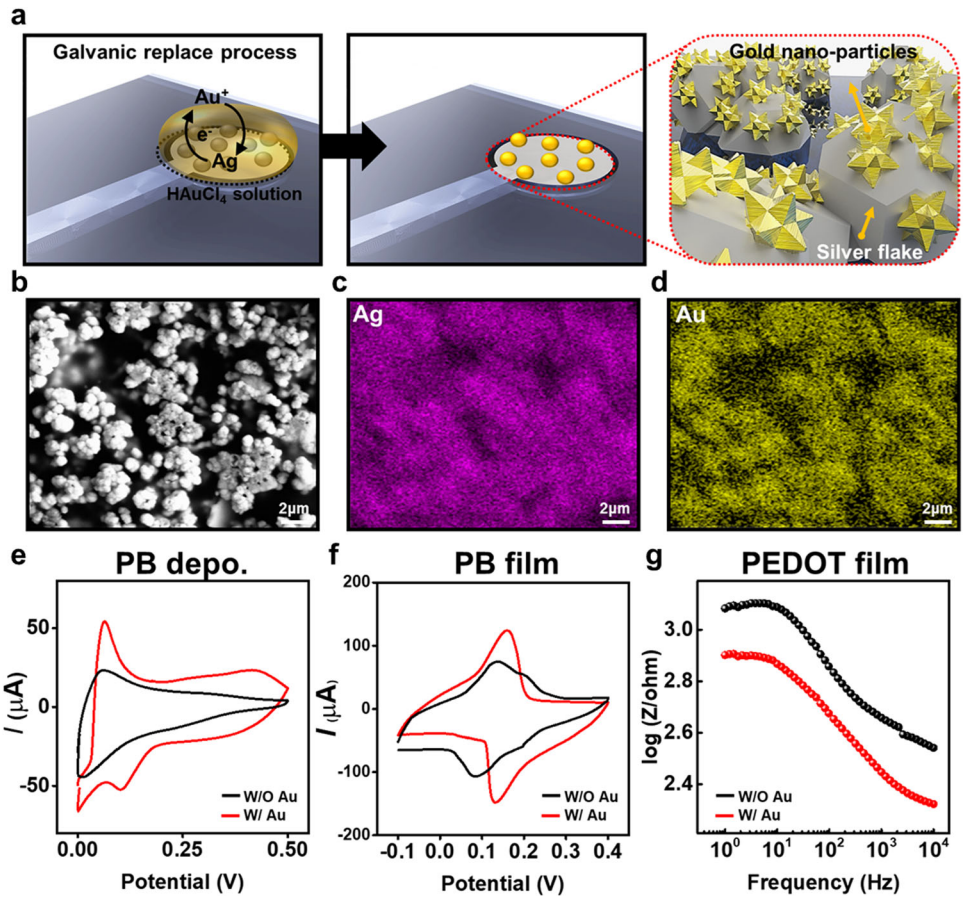

Fig. 2 Au modified Ag electrode via galvanic replacement process to enhance electrochemical properties. a Schematic drawing of galvanic replacement process on the Ag electrode. **b** SEM image of Ag electrode comprised with Ag flakes and Ecoflex. **c** EDS image of Ag flakes in Ecoflex matrix. **d** EDS image of AuNPs formed by galvanic replacement process. **e** CV plots of the electrodes during PB electrodeposition (scan rate: 0.1 V s^{-1} with a commercial Ag/AgCl electrode). **f** CV plots of the electrodes in PBS with $Fe(CN)_6^{3-/4-}$ after electrodeposition of PB (scan rate: 0.1 V s^{-1} from −0.1 V to 0.4 V with a commercial Ag/AgCl electrode). **g** Site impedance of the electrode in PBS with $Fe(CN)_6^{3-/4-}$ after electrodeposition of PEDOT.

(Fig. 3b). Ecoflex was used as the components for stretchable circuit including substrate, nanocomposite conductor and encapsulation layer. The stretchable electrode combined with Ecoflex could provide the high conformity and stretchability that are desired for wearable devices[49]. In multi-biochemical sensors, it is essential to prevent electrical interference between different sensor elements or components. The PPE encapsulation layer acts as an insulating barrier, effectively isolating the various components from each other. In detail (Fig. 3c, d, Supplementary Fig. 9), Photo-patternable Ecoflex (PPE) was directly patterned on the stretchable conductor to serve as the encapsulation layer that enables selective sensing of diverse biomarkers without crosstalk (Supplementary Fig. 10). Then AuNps was coated onto opened silver nanocomposite conductor to enhance the electrochemical properties of electrode. The working electrodes were functionalized by electrodeposition to fabricate each independent biochemical sensors[50]. The multi-biochemical sensor consisted of components to sense glucose, lactate, pH and humidity independently (Fig. 3c). Each sensing part functions as a distinct working electrode to non-invasively monitor a specific component of sweat. The reference electrode is composed of Ag/AgCl to ensure stable electrochemical sensing. The sweat sensor is fabricated in as a wrist patch to enable conformal contact with skin (Fig. 3e–f). Detailed fabrication process of stretchable sensor is shown in Supplementary Fig. 11.

Assessment of stretchable sensors for multiple biomarkers

The stretchable biochemical sensors achieved multi-sensing (Fig. 4a–p), both in their normal state and under mechanical deformation to 50% tensile strain. The stretchable sensor's characteristics were assessed by subjecting it to tensile strength while securing both ends. To ensure precise strain application, the sensor's characteristics were evaluated by manually applying a tensile strength after securing it with PI tape on the 1-axis stage (Supplementary Fig. 12). The humidity sensor (Fig. 4a) was fabricated using a PEDOT electrode. In the presence of PBS, the impedance of the electrode decreased by two orders of magnitude (Fig. 4b). The humidity sensor showed a stable impedance regardless of applied strain up to 50% (Fig. 4c). The normalized sensitivity of the humidity sensor was constant for 1000 cycles to 20% strain (Fig. 4d).

The pH sensor (Fig. 4e) was composed of polyaniline (PANi) due to its changes of surface protonation at different pH levels. A standard pH buffer solution was used to calibrate the pH sensor. The open circuit voltage (OCP) of the pH sensor decreased stepwise as pH increased (Fig. 4f). During 30 s at each pH level, and signal of the pH sensor varied by <0.1 V. The pH sensor operated stably under deformations (Fig. 4g), and the response was stable performance after during cyclic stretching at 20% tensile strain (Fig. 4h).

The electrochemical sensor for lactate (Fig. 4i) used an enzyme. This sensor was evaluated in vitro. The current through the sensor reached equilibrium within seconds. The magnitude of the

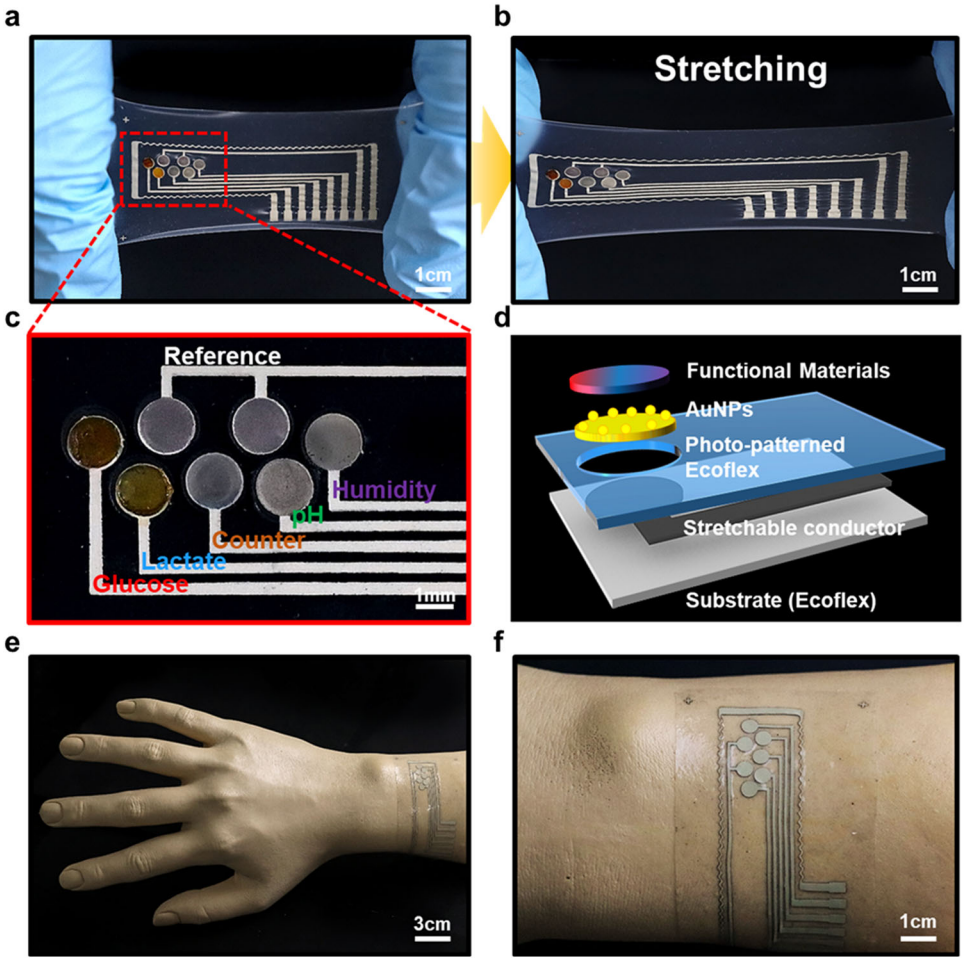

Fig. 3 Intrinsically stretchable multi-biochemical sensor monitoring analytes in sweat. a, **b** Illustration of the stretchable sensor for sweat analysis. **c** Photograph of the stretchable multi-electrochemical sensor array. **d** Schematic illustration of all components for stretchable wearable patch including photo-patterned Ecoflex and functional materials. **e**, **f** Schematic image of intrinsically stretchable multi-biochemical sensor placed on a wrist.

(negative) equilibrium current increased as lactate concentration increased in the range of 1–15 mM (Fig. 4j). The normalized sensitivity decreased by only ~10% when the sensor was estimated while stretched to 50% (Fig. 4k). The sensor also showed good durability in the cyclic stretching test (Fig. 4l).

The electrochemical sensor for glucose (Fig. 4m) also used an enzyme. This sensor was also evaluated in vitro. The magnitude of the (negative) equilibrium current increased as glucose concentration increased in the range of 0.1 to 0.5 mM (Fig. 4n), and showed constant sensitivity under deformation (Fig. 4o), and during repetitive stretching test (Fig. 4p).

The lactate and glucose sensors did not suffer from cross-talk (Supplementary Fig. 10), i.e., they showed good selectivity for certain target biomarkers in the presence of other biomolecules and drugs. Compared with the current of the target analytes, that of other biomarkers represents an undetectable value. These results show that these four electrochemical sensors have stable sensitivity and selectivity under harsh deformation circumstances, and therefore have potential for efficient detection of biomarkers in sweat.

Stretchable sweat patch for real-time sweat analysis

We evaluated the stretchable sweat sensing patch in real time. A hydrophilic sweat-uptake layer was placed on the arm to efficiently absorb a sufficient amount of sweat (Supplementary Fig. 13). The patch was laminated on the arm of a volunteer (Fig. 5a), and connected to an electrochemical analyzer that collected and transmitted the data. Given the minor sensitivity changes observed when strain is applied to the stretchable sweat patch, we fabricated a strain sensor to counteract this effect (Supplementary Fig. 14). To ensure reliable measurements, we created three different strain sensors and then evaluated their linearity. The resistance of the strain sensor, constructed using a wavy-patterned electrode, was found to increase linearly, showing a proportional relationship with strain. This strain sensor calibrates any strain that could transpire when a volunteer is wearing the stretchable sweat patch, providing more accurate results. The volunteer was asked to perform stationary cycling at a fixed rate for 30 min to produce sufficient sweat for analysis. To identify the influence of food intake, the glucose level was recorded in a fasting state and after food intake. The patch enabled real-time monitoring of the glucose level in the sweat of the volunteer (Fig. 5b). The glucose level was quantified as 70 mg/dl in the fasting state and 100 mg/dl after food intake. The results of our stretchable sweat patch are consistent with those from a commercial glucose-assay kit assay (Fig. 5c). To continuously evaluate the sweat lactate level, the analysis was conducted before, during and after exercise (Fig. 5d). The volunteer was asked to cycle for 30 min to collect the sweat. The lactate level was estimate from 5 to 16 mM during exercise. The sweat lactate level obtained using the wearable sweat patch was consistent with measurements obtained using a blood lactate meter (Fig. 5e).

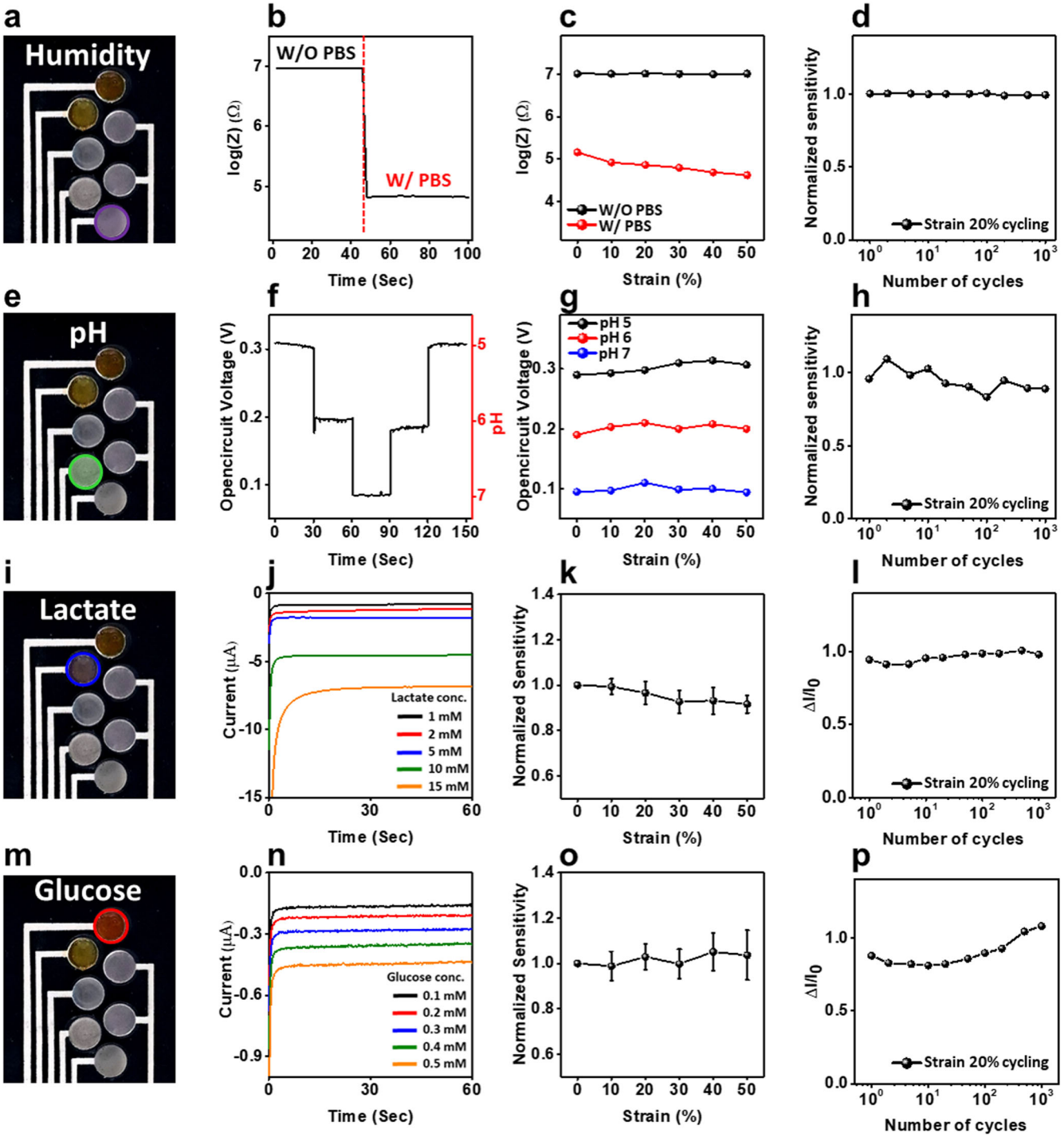

Fig. 4 Electrochemical and electrical characterization of individual sensor and their combined operation in vitro. a–d Characterization of humidity sensor. **b** Measurement of impedance change of PEDOT with PBS. **c** Measurement of impedance change of PEDOT when stretched up to 50%. **d** Cycling test of humidity sensor after every 20% strain up to 1000 cycles. **e–h** Characterization of pH sensor. **f** Measurement of open circuit voltage change depending on pH value of PBS. **g** Measurement of open circuit voltage of pH sensor when stretched up to 50%. **h** Cycling test of pH sensor after every 20% strain up to 1,000 cycles. **i-l** Characterization of lactate sensor. **j** Amperometric measurements using PB modified working electrode with redox enzyme, lactate oxidase. **k** Normalized sensitivity of the lactate sensor when stretched up to 50%. Data are presented as mean ± SD. ($n = 3$) **l** Cycling test of lactate sensor after every 20% strain up to 1000 cycles. **m–p** Characterization of glucose sensor. **n** Amperometric measurement of glucose sensor. **o** Normalized sensitivity of the glucose sensor when stretched up to 50%. Data are presented as mean ± SD. ($n = 3$) **p** Cycling test of glucose sensor after every 20% strain up to 1000 cycles.

METHODS

Preparation of materials

Ecoflex 00-30 and SLO-JO was purchased from Smooth-on. Silver flakes (DSF-500MWZ-S) were purchased from Daejoo Electronics. Benzophenone, 3,4-Ethylenedioxythiophene (EDOT), Lithium perchlorate (LiClO4), acetonitrile, aniline, chitosan, acetic acid, bovine serum albumin, ectoine, L-latic acid, D+ glucose, Nafion, glutaraldehyde, hydrochloric acid (HCl), sodium chloride (NaCl),

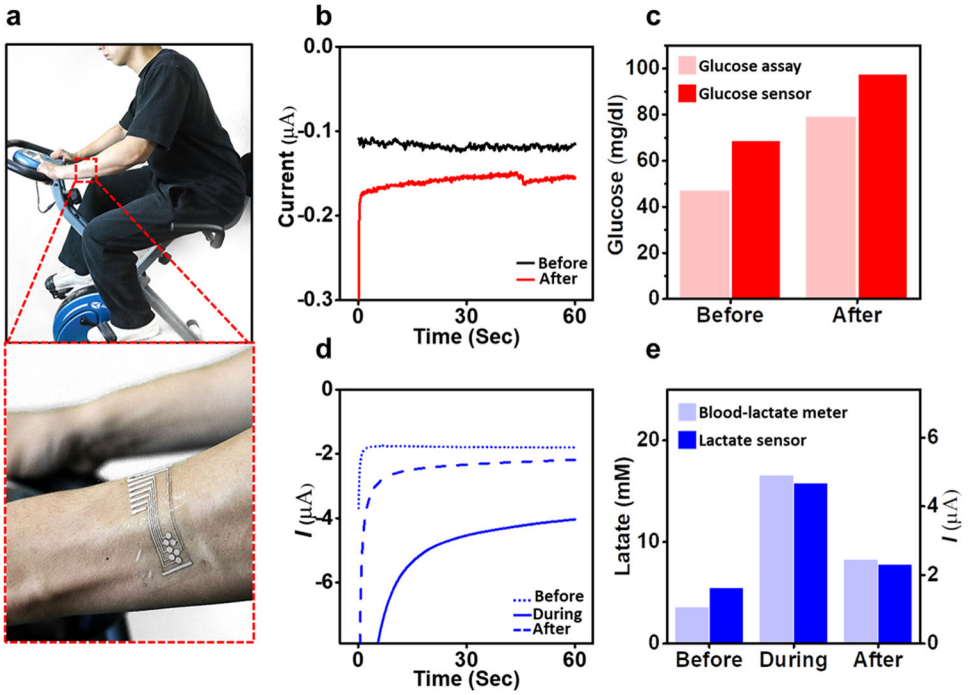

Fig. 5 On-body evaluation of stretchable sweat sensor for real-time monitoring. a Photograph of the sweat-analysis sensor attached on the arm of a volunteer for continuous on-body monitoring the biomarkers. **b** Real-time recording of sweat glucose before and after intake of meal. **c** Comparison of the sweat glucose concentrations measured by the sweat sensor and commercial glucose-assay kit. **d** Real-time recording of sweat lactate before, during and after exercise. **e** Comparison of the sweat lactate concentrations measured by the sweat sensor and commercial blood-lactate meter. Note that the commercial blood-lactate meter was used to identify a variation in lactate level during exercise, not to measure sweat lactate level[28].

potassium chloride (KCl), potassium ferricyanide (III), Iron(III) chloride hexahydrate, ammonium hydroxide solution, glucose assay kit, phosphate buffered saline tablet, Acetaminophen, Acetylsalicylic acid, L-Ascorbic acid, Uric acid, aniline, Gold(III) chloride trihydrate, chloroplatinic acid hexahydrate, 4-Methyl-2-pentanone were obtained from Sigma-Aldrich. GOx (GLO-201) and LOx (LCO-301) were purchased from TOYOBO chemical. Dulbecco's Modified Eagle's Medium (DMEM), fetal bovine serum (FBS), antibiotic-antimycotic (AA), and LIVE/DEAD assay kit were obtained from Invitrogen (USA). CCK-8 assay kit bought from Dojindo (Japan).

Fabrication of the Ag electrode

A stretchable elastic conductor was fabricated from Ag ink composed of Ecoflex, silver flakes and methyl isobutyl ketone (MIBK). The prepolymer (Ecoflex-A) and cross-linker (Ecoflex-B) of Ecoflex were mixed in a 1:1 (w/w) ratio for 5 min by a paste mixer, then MIBK was slowly added over a period of 5 min. The mixing weight ratio of Ag flakes: Ecoflex: MIBK was 7.2: 1.6: 1.5. All components were mixed using a magnetic stirrer for 3 h at room temperature. The screen-printing was performed using Ag ink on the Ecoflex substrate. The printed Ag ink was cured at 60 °C for 1 h, then at 120 °C for 2 h.

Patterning of the photo-patternable ecoflex

To prepare PPE, benzophenone was dissolved at 1:1 (w/w) ratio in xylene, then 4 wt% of the prepared solution was mixed with Ecoflex prepolymer. SLO-JO was added 1 wt% of solution. PPE was spin-coated on the Ecoflex substrate at 700 rpm for 60 s. Then the PPE was exposed to UV light at 365 nm by using a xenon-mercury UV lamp (Thermo Oriel, 69910, 1.2 mW/cm^2) for 10 min, then PPE-annealed on a hot plate at 85 °C for 1 min. The unexposed region was developed using MIBK solution for 1 min, then the surface was rinsed and cleaned using isopropanol (IPA). Finally, the sample was cured at 100 °C for 1 h.

Biocompatibility evaluation

L929 mouse skin fibroblast cells and its complete growth medium (DMEM, 10% FBS, 1% AA) were employed for verifying the biocompatilbity of developed Photo-patternable Ecoflex (PPE) film. LIVE/DEAD and CCK-8 assay evaluations were performed with reference to the literature[51]. To acquire CCK-8 and LIVE/DEAD assay results, sterilized PPE films were placed in a 96-wall polystyrene cell culture plates with 2000 cells and a polystyrene cell culture dish with 40,000 cells, respectively. After 1 and 3 days of culture, CCK-8 assay results were collected by a microplate reader (Victor 3, PerkinElmer, USA) by measuring optical absorbance at 450 nm. Also, LIVE/DEAD assay and bright-field images were captured by an optical microscope (Eclipse 80i, Nikon, Japan) equipped with a digital single-lens reflex camera (DS-Ri2, Nikon, Japan).

Resistance measurement of stretchable Ag conductor

The resistance of stretchable Ag conductor was measured using a multi-meter (Hioki 3803) while strain was applied using translation stage. Thin copper wire was connected to contact pads with PI tape.

Electrode modification

The galvanic replacement process was used to modify the Ag electrode. A solution of 0.3 mM Gold (III) chloride trihydrate ($HAuCl_4{\cdot}3H_2O$) in DI water was prepared. The Ag electrode was dipped into the solution for 10 min, then rinsed with a 28% aqueous solution of ammonia (NH_4OH) to remove the byproduct of the galvanic replacement. A solution of 3 mM chloroplatinic acid hexahydrate ($H_2PtCl_6{\cdot}6H_2O$) in DI water was prepared. The

counter electrode was immersed in this solution for 10 min. The modified electrode was washed with an aqueous solution of NH_4OH.

Functionalization of the electrochemical multi sensor

Electrodeposition was used to functionalize selective materials on the desired site without cross-contamination. Prussian blue electrodeposition. An aqueous solution of 10 mM KCl, 2.5 mM $K_3[Fe(CN)_6]$ and 2.5 mM $FeCl_3{\cdot}6H_2O$ in 0.1 M HCl was prepared. The Au-modified Ag electrode was dipped in the solution, and the potential was swept from 0 to 0.5 V versus a commercial Ag/AgCl for two segments for the glucose sensor. The deposition process involved applying a voltage range from −0.5 V to 0.6 V (versus Ag/AgCl) for 10 segments at a scan rate of 50 mV s^{-1} for the lactate sensor.

For PANi electrodeposition, an aqueous solution of 0.1 M aniline in 1 M HCl was prepared. The Au-modified Ag electrode was immersed in the solution, then the potential was swept from −0.2 to 1 V versus a commercial Ag/AgCl electrode for 50 segments at a scan rate of 0.1 V s^{-1}.

For the PEDOT deposition, a solution of 0.01 M 3,4-ethylenedioxythiophene and 0.1 M $LiClO_4$ in acetonitrile was prepared. The Au-modified Ag electrode was immersed in the solution, then galvanostatic electrodeposition was performed for 60 s at 1.2 V (potential versus commercial Ag/AgCl electrode).

Biosensor modification

A chitosan solution was prepared by dissolving 0.5 wt% of chitosan in 0.1 M acetic acid. For preparing the glucose sensor, the chitosan solution was mixed with GOx (50 mg/mL), bovine serum albumin (15 mg/mL) and ectoine (15 mg/mL), then 1.5 µL of the mixed solution was drop-cast onto the working electrode. To prepare the lactate sensor, the chitosan solution was mixed with LOx (50 mg/mL) and bovine serum albumin (15 mg/mL), then 1.5 µL of the mixed solution was drop-cast onto the working electrode.

The working electrodes were dried under ambient conditions, then 1 µL of 0.5 wt% Nafion was drop-cast on the enzyme-modified surfaces, then allowed to dry at room temperature for 1 h. Then 1 µL of 1 wt% of glutaraldehyde was dropcast onto the working electrode.

In vitro characterization of the multi sensors

An electrochemical analyzer (CHI660E, CHI instruments) was used to characterize and calibrate all sensors. The humidity sensor was calibrated using AC impedance measurement, using the two-electrode method. A PEDOT-modified working electrode and Ag/AgCl modified counter electrode were used for the humidity sensor. The calibration curve was obtained by measuring the impedance change in an artificial sweat solution.

The pH sensor was calibrated using open-circuit potential measurement. PANi and Ag/AgCl modified electrodes were used for the pH measurement. The calibration curve was obtained by using standard buffered pH solution (pH 4–6, Alfa Aesar). The electrochemical sensor was calibrated in 0.1 M phosphate-buffered saline (PBS) (pH 7.0) with a change in the concentration of the analyte. Chronoamperometry was used for the electrochemical detection of hydrogen peroxide to determine the glucose and lactate concentration. The calibration curve was obtained for 60 s with an initial potential of −0.1 V (versus Ag/AgCl).

On-body evaluation for the sweat analysis

On-body evaluation of the device was performed on a healthy subject who had no history of diabetes or chronic pain. The measurements were collected in strict compliance with a protocol approved by the institutional review board at Korea Advanced Institute Science and Technology (IRB No.kh2021-184). A sweat-uptake layer (wood pulp and Rayon, SWISSPURE half sponge sheet, Able C&C) was integrated with wearable device for efficient sweat collection. The sweat analysis patch was attached to the arm of the volunteer for on-body evaluations. The glucose and lactate signals were validated with a commercial glucose assay kit (GAGO20, Sigma-aldrich) and blood-lactate meter (LT-1730, Arkray) respectively, before measurements using the sweat analysis patch. The volunteer was asked to ride a stationary bicycle for sweat collection. For the electrochemical measurement, the sweat monitoring patch is connected to an electrochemical analyzer (CHI660E, CHI instruments) via flexible electric wires.

Strain sensor

The strain sensor was made with an Ag electrode via screen printing. It was patterned as a thin and wavy shape in a horizontal direction. It was patterned thickly to minimize the effect of longitudinal deformation. Calibration was carried out by using PBS solution of glucose and lactate.

Tensile and peel test

The tensile properties were evaluated using a universal testing machine (AGS-X, Japan). Dogbone-shaped specimen was prepared with a gauge section with 2 mm width and length of 10-mm. The test speed of the crosshead was 10 mm/min in engineering strain rate. Samples were pneumatically held during the experiment to prevent slipping. The elastic modulus was determined from the slope of the stress-strain curve from the elastic region during the initial loading. The peel test was conducted using a universal testing machine (AGS-X, Japan). Rectangular shaped specimen was prepared with 10 mm width and length of 60 mm. This test involves sandwiching a sample of the material between two surfaces (180 degree) and then peeling them apart at a controlled rate (100 mm/min).

DATA AVAILABILITY

The data that support the findings of this study are available from the corresponding author upon reasonable request.

Received: 27 February 2023; Accepted: 16 July 2023;
Published online: 24 July 2023

REFERENCES

1. Song, E. et al. Ultrathin trilayer assemblies as long-lived barriers against water and ion penetration in flexible bioelectronic systems. *ACS Nano* **12**, 10317–10326 (2018).
2. Bandodkar, A. J., Jeang, W. J., Ghaffari, R. & Rogers, J. A. Wearable sensors for biochemical sweat analysis. *Ann. Rev. Anal. Chem.* **12**, 1–22 (2019).
3. Sang, M., Kim, K., Shin, J. & Yu, K. J. Ultra-thin flexible encapsulating materials for soft bio-integrated electronics. *Adv. sci.* **9**, 2202098 (2022).
4. Song, J., Feng, X. & Huang, Y. Mechanics and thermal management of stretchable inorganic electronics. *Natl Sci. Rev.* **3**, 128–143 (2015).
5. Yuk, H. et al. Dry double-sided tape for adhesion of wet tissues and devices. *Nature* **575**, 169–174 (2019).
6. le Floch, P. et al. Fundamental limits to the electrochemical impedance stability of dielectric elastomers in bioelectronics. *Nano Lett.* **20**, 224–233 (2020).
7. Bariya, M., Nyein, H. Y. Y. & Javey, A. Wearable sweat sensors. *Nat. Electron.* **1**, 160–171 (2018).
8. Sempionatto, J. R. et al. Epidermal enzymatic biosensors for sweat Vitamin C: Toward personalized nutrition. *ACS Sens* **5**, 1804–1813 (2020).
9. Li, H., Ma, Y. & Huang, Y. Material innovation and mechanics design for substrates and encapsulation of flexible electronics: a review. *Mater. Horiz.* **8**, 383–400 (2021).
10. Kim, D. H. et al. Epidermal electronics. *Science* **333**, 838–843 (2011).
11. Wang, C., Wang, C., Huang, Z. & Xu, S. Materials and structures toward soft electronics. *Adv. Mater.* **30**, 1801368 (2018).
12. Oh, Y. S. et al. Battery-free, wireless soft sensors for continuous multi-site measurements of pressure and temperature from patients at risk for pressure injuries. *Nat. Commun.* **12**, 5008 (2021).

13. Kathe, C. et al. Wireless closed-loop optogenetics across the entire dorsoventral spinal cord in mice. *Nat. Biotechnol.* **40**, 198–208 (2022).
14. Zhai, Q. et al. Vertically aligned gold nanowires as stretchable and wearable epidermal ion-selective electrode for noninvasive multiplexed sweat analysis. *Anal. Chem.* **92**, 4647–4655 (2020).
15. Xu, Y. et al. Multiscale porous elastomer substrates for multifunctional on-skin electronics with passive-cooling capabilities. *Proc. Natl. Acad. Sci. USA* **117**, 205–213 (2020).
16. Li, H. et al. Breathable and skin-conformal electronics with hybrid integration of microfabricated multifunctional sensors and kirigami-structured nanofibrous substrates. *Adv. Funct. Mater.* **32**, 2202792 (2022).
17. Wang, S. et al. Skin electronics from scalable fabrication of an intrinsically stretchable transistor array. *Nature* **555**, 83–88 (2018).
18. Bandodkar, A. J., Nuñez-Flores, R., Jia, W. & Wang, J. All-printed stretchable electrochemical devices. *Adv. Mater.* **27**, 3060–3065 (2015).
19. Kim, Y. S. et al. Soft wireless bioelectronics designed for real-time, continuous health monitoring of farmworkers. *Adv. Healthc. Mater.* **11**, 2200170 (2022).
20. Kim, T., Yi, Q., Hoang, E. & Esfandyarpour, R. A 3D printed wearable bioelectronic patch for multi-sensing and in situ sweat electrolyte monitoring. *Adv. Mater. Technol.* **6**, 2001021 (2021).
21. Kim, J., Campbell, A. S., de Ávila, B. E. F. & Wang, J. Wearable biosensors for healthcare monitoring. *Nat. Biotechnol.* **37**, 389–406 (2019).
22. Gao, W. et al. Wearable microsensor array for multiplexed heavy metal monitoring of body fluids. *ACS Sens* **1**, 866–874 (2016).
23. Choi, J. et al. Soft, skin-integrated multifunctional microfluidic systems for accurate colorimetric analysis of sweat biomarkers and temperature. *ACS Sens* **4**, 379–388 (2019).
24. Zhang, S. et al. Hydrogel-enabled transfer-printing of conducting polymer films for soft organic bioelectronics. *Adv. Funct. Mater.* **30**, 1906016 (2020).
25. Wang, L., Xu, T., He, X. & Zhang, X. Flexible, self-healable, adhesive and wearable hydrogel patch for colorimetric sweat detection. *J. Mater. Chem. C.* **9**, 14938–14945 (2021).
26. Lee, C. et al. Bioinspired, calcium-free alginate hydrogels with tunable physical and mechanical properties and improved biocompatibility. *Biomacromolecules* **14**, 2004–2013 (2013).
27. Toi, P. T., Trung, T. Q., Dang, T. M. L., Bae, C. W. & Lee, N. E. Highly electrocatalytic, durable, and stretchable nanohybrid fiber for on-body sweat glucose detection. *Acs. Appl. Mater. Interfaces* **11**, 10707–10717 (2019).
28. Sempionatto, J. R. et al. An epidermal patch for the simultaneous monitoring of haemodynamic and metabolic biomarkers. *Nat. Biomed. Eng.* **5**, 737–748 (2021).
29. Natarajan, S., Chang-Yen, D. & Gale, B. Large-area, high-aspect-ratio SU-8 molds for the fabrication of PDMS microfluidic devices. *J. Micromech. Microeng.* **18**, 045021 (2008).
30. Tringides, C. M. et al. Viscoelastic surface electrode arrays to interface with viscoelastic tissues. *Nat. Nanotechnol.* **5**, 1019–1029 (2021).
31. Wolfe, D. B. et al. Customization of poly(dimethylsiloxane) stamps by micromachining using a femtosecond-pulsed laser. *Adv. Mater.* **15**, 62–65 (2003).
32. Kim, T., Kim, D. M., Lee, B. J. & Lee, J. Soft and deformable sensors based on liquid metals. *Sensors* **19**, 4250 (2019).
33. Bhagat, A. A. S., Jothimuthu, P. & Papautsky, I. Photodefinable polydimethylsiloxane (PDMS) for rapid lab-on-a-chip prototyping. *Lab Chip* **7**, 1192–1197 (2007).
34. Kang, J. et al. Photopatternable poly(dimethylsiloxane) (PDMS) for an intrinsically stretchable organic electrochemical transistor. *Acs. Appl. Mater. Interfaces* **14**, 24840–24849 (2022).
35. Pan, S. et al. Mechanocombinatorially screening sensitivity of stretchable strain sensors. *Adv. Mater.* **31**, 1903130 (2019).
36. Kim, S. H. et al. Ultrastretchable conductor fabricated on skin-like hydrogel–elastomer hybrid substrates for skin electronics. *Adv. Mater.* **30**, 1800109 (2018).
37. Shyu, T. C. et al. A kirigami approach to engineering elasticity in nanocomposites through patterned defects. *Nat. Mater.* **14**, 785–789 (2015).
38. Wan, D., Xia, X., Wang, Y. & Xia, Y. Robust synthesis of gold cubic nanoframes through a combination of galvanic replacement, gold deposition, and silver dealloying. *Small* **9**, 3111–3117 (2013).
39. Patel, D. K. et al. Highly stretchable and UV curable elastomers for digital light processing based 3D printing. *Adv. Mater.* **29**, 1606000 (2017).
40. Basu, M. et al. Hydroxylation of benzophenone with ammonium phosphomolybdate in the solid state via UV photoactivation. *Chem. Commun.* **46**, 7191–7193 (2009).
41. Li, J. et al. Correlations between percolation threshold, dispersion state, and aspect ratio of carbon nanotubes. *Adv. Funct. Mater.* **17**, 3207–3215 (2007).
42. Kim, S. H. et al. An ultrastretchable and self-healable nanocomposite conductor enabled by autonomously percolative electrical pathways. *ACS Nano* **13**, 6531–6539 (2019).
43. Matsuhisa, N. et al. High-transconductance stretchable transistors achieved by controlled gold microcrack morphology. *Adv. Electron. Mater.* **5**, 1900347 (2019).
44. Nasraoui, S. et al. Electrochemical sensor for nitrite detection in water samples using flexible laser-induced graphene electrodes functionalized by CNT decorated by Au nanoparticles. *J. Electroanal. Chem.* **880**, 114893 (2021).
45. Dakshayini, B. S. et al. Role of conducting polymer and metal oxide-based hybrids for applications in ampereometric sensors and biosensors. *Microchem. J.* **147**, 7 (2019).
46. Kim, H. J., Sim, K., Thukral, A. & Yu, C. Rubbery electronics and sensors from intrinsically stretchable elastomeric composites of semiconductors and conductors. *Sci. Adv.* **3**, el701114 (2017).
47. Gao, W. et al. Fully integrated wearable sensor arrays for multiplexed in situ perspiration analysis. *Nature* **529**, 509–514 (2016).
48. Chen, R. et al. Use of platinum as the counter electrode to study the activity of nonprecious metal catalysts for the hydrogen evolution reaction. *ACS Energy Lett.* **2**, 1070–1075 (2017).
49. Matsuhisa, N. et al. Printable elastic conductors with a high conductivity for electronic textile applications. *Nat. Commun.* **6**, 7461 (2015).
50. Lee, H. et al. A graphene-based electrochemical device with thermoresponsive microneedles for diabetes monitoring and therapy. *Nat. Nanotechnol.* **11**, 566–572 (2016).
51. Jang, J. & Park, C. B. Magnetoelectric dissociation of Alzheimer's Beta-amyloid aggregates. *Sci. Adv.* **8**, eabn1675 (2022).

ACKNOWLEDGEMENTS

This work was supported by the Wearable Platform Materials Technology Center (WMC) funded by the National Research Foundation of Korea (NRF) grant by the Korea Government (MSIT) (NRF-2022R1A5A6000846, NRF-2021M3D1A2049869, NRF-2020M3H4A3106405). This research was also supported by Nano Material Technology Development Program (2021M3H4A1A04092879) through the National Research Foundation of Korea funded by the Ministry of Science and ICT.

AUTHOR CONTRIBUTIONS

W.L. and B.-S.B. proposed the concept and designed the experiment. S.K. carried out most of the experiment with the help from other co-authors. J.K. and I.L. participated in the fabrication and electrochemical characterization of the sensors. J.J. and C.B.P. contributed to biocompatibility evaluation. All authors discussed the result and contributed to proofreading the manuscript.

COMPETING INTERESTS

The authors declare no conflict of interest.

ADDITIONAL INFORMATION

Supplementary information The online version contains supplementary material available at https://doi.org/10.1038/s41528-023-00268-x.

Correspondence and requests for materials should be addressed to Wonryung Lee or Byeong-Soo Bae.

Reprints and permission information is available at http://www.nature.com/reprints

Publisher's note Springer Nature remains neutral with regard to jurisdictional claims in published maps and institutional affiliations.

Open Access This article is licensed under a Creative Commons Attribution 4.0 International License, which permits use, sharing, adaptation, distribution and reproduction in any medium or format, as long as you give appropriate credit to the original author(s) and the source, provide a link to the Creative Commons license, and indicate if changes were made. The images or other third party material in this article are included in the article's Creative Commons license, unless indicated otherwise in a credit line to the material. If material is not included in the article's Creative Commons license and your intended use is not permitted by statutory regulation or exceeds the permitted use, you will need to obtain permission directly from the copyright holder. To view a copy of this license, visit http://creativecommons.org/licenses/by/4.0/.

© The Author(s) 2023